Effect of the Dynamics of the MTDC Power System on DC Voltage Oscillation Stability

Qiang Fu, *Member, IEEE*, Wenjuan Du, *Member, IEEE*, Haifeng Wang, *Senior Member, IEEE*, and Xianyong Xiao, *Senior Member, IEEE*

***Abstract*—Ignoring parts of the dynamics of a multiterminal DC (MTDC) power system can simplify its stability analysis but may miss some instability risks in the analyzed results. This study analyzed the stability of DC voltage oscillation by considering comprehensive dynamics of an MTDC system in a DC voltage time scale to reveal the stability mechanism of the DC voltage oscillation accurately. It demonstrated that a DC voltage oscillation loop is first formed by the DC voltage control of the voltage source converter (VSC). Subsequently, it is affected by the dynamics of the remaining DC system (RDCS) through two paths: (1) the equivalent conductance of the RDCS is equal to an additional damping added to the DC voltage oscillation loop, and (2) the equivalent susceptance forms a mirrored subsystem and results in an open-loop modal resonance, which always induces negative effects on DC voltage oscillation stability. These conclusions are also correct in parts of the MTDC system using DC voltage droop control. Moreover, a method was proposed to quickly determine the stable operating region of the RDCS. Finally, accuracy of the stability mechanism of the DC voltage oscillation and effectiveness of the proposed method are verified based on the SIMULINK platform.**

***Index Terms*—DC voltage oscillation, MTDC power system, stability mechanism analysis, VSC.**

NOMENCLATURE

C_k	Capacitance on the DC side of the k^{th} VSC
$\bar{V}_k$	DC voltage of the k^{th} VSC
$\bar{I}_{netk}$	DC current at input C_k from the DC network
$\bar{I}_k$	DC current at output of C_k
X_k	Reactance of the filter on the AC side of the k^{th} VSC
$\tilde{I}_{dk}$	AC current in the d axis
$\tilde{I}_{qk}$	AC current in the q axis
P_k	Active power at the output of the k^{th} VSC
$\tilde{V}_k$	AC voltage at the point of common coupling
$\tilde{V}_{dk}$	d-axis component of $\tilde{V}_k$
$\tilde{V}_{qk}$	q-axis component of $\tilde{V}_k$
$\tilde{V}_{ck}$	AC voltage at the terminal of the AC–DC converter
$\tilde{V}_{cdk}$	d-axis component of $\tilde{V}_{ck}$
$\tilde{V}_{cqk}$	q-axis component of $\tilde{V}_{ck}$
ω_0	Synchronous frequency, 377 rad/s
$K_{pk} + K_{ik}s^{-1}$	Transfer function of the outer control loop of the k^{th} VSC
$K^c_{pk} + K^c_{ik}s^{-1}$	Transfer function of the inner control loop of the k^{th} VSC
Superscript *ref*	Reference value of the control system
Subscript k	Number identifier of all VSCs
Subscript j	Number identifier of the active power-controlled VSCs
ω_d	Frequency of DC voltage oscillation
D_d	Damping of DC voltage oscillation
g_{net}	Equivalent conductance of RDCS
b_{net}	Equivalent susceptance of RDCS
Δ	Small increment in variable
$\|\|$	Absolute value of variable
$\mathbf{E}$	Identity matrix
$\mathbf{0}$	Zero matrix
Superscript $'$	Orthogonal direction of the variable
Subscript N	Total number of DC nodes
Im	Imaginary part of the complex number
Re	Real part of the complex number.

Manuscript received 27 January 2021; revised 16 June 2021, 12 September 2021, and 24 November 2021; accepted 6 January 2022. Date of publication 21 January 2022; date of current version 19 August 2022. This work was supported in part by the Engineering Special Team of Sichuan University on New Energy Power Systems, in part by the Natural Science Foundation of China under Grant 52077144, and in part by the Youth Innovative Research Team of Science and Technology Scheme under Grant 22CXTD0066 New Energy Power System, Sichuan Province, China. Paper no. TPWRS-00146-2021. *(Corresponding author: Wenjuan Du.)*

The authors are with the Sichuan University, Wangjiang Campus, Chengdu 610017, China (e-mail: fuqiang346@qq.com; ddwenjuan@qq.com; hfwang60@qq.com; xiaoxianyong@163.com).

Color versions of one or more figures in this article are available at https://doi.org/10.1109/TPWRS.2022.3144388.

Digital Object Identifier 10.1109/TPWRS.2022.3144388

I. INTRODUCTION

MULTITERMINAL DC (MTDC) network technology is one of the best technologies for transmitting wind power [1]. However, the small-signal stability of MTDC power systems is a vital issue that needs to be examined carefully, and in recent years, it has received considerable interest from power system researchers and engineers [1], [2].

The stability of DC voltage oscillations is a major issue that has been investigated actively in recent years. So far, two main problems have been identified related to the small-signal DC voltage stability for VSC-MTDC power systems. The first problem is the instability caused by the dynamic interaction between AC and DC power systems. Studies addressing this problem assumed that the independent AC and DC power systems were stable; however, integrating AC and DC power systems can

induce instability problems [3]–[6] because the dynamic interaction between AC and DC power systems has a negative effect on the stability of the AC/DC hybrid power system. The second problem is the instability caused by the dynamic interactions between voltage source converters (VSCs) and the DC network [7]–[10] in a standalone DC power system. The stability of DC voltage oscillations as a stability issue in a standalone DC power system has gained considerable research attention. To evaluate how DC dynamics affect the stability of the DC power system, the dynamics of the AC power system were excluded, and the AC power system was represented using an infinite bus. This study focuses on the second problem.

Currently, frequency domain analysis and modal analysis have been adopted to examine the small-signal stability of MTDC power systems. These studies demonstrated and validated the instability risk caused by the VSCs, which is related to DC voltage oscillations [5], [6], [10]. However, DC networks and equipment are considered as resistive to simplify the stability analysis of the MTDC power system. For example, [11] established a linearized model of the MTDC power system without considering the dynamics of DC transmission lines, and therefore the transfer function between DC currents and voltages was linear, which simplified the complexity of the DC network. In [12], the dynamics of DC transmission lines were excluded to investigate the stability of the MTDC power system. The effect of DC network dynamics appears to be weak because many studies confirm that ignoring these dynamics rarely affects the simulated and analyzed results [11], [12]. However, the generalization of the above conclusion has not been verified in theory, and there is no clarity on how the dynamics of the DC network affect the stability of the MTDC power system. Furthermore, some studies consider DC equipment as resistance or constant power to simplify the MTDC power system. In [13], the grid-side converter dynamics are excluded from the DC system dynamics and were represented by a constant DC voltage source instead. In [14], the converters were simplified as constant power loads to investigate the effect of parallel-connected VSCs on the stability of the MTDC power system. Similar to [14] and [15], VSCs are considered as constant power sources when analyzing the DC voltage stability for DC transmission systems.

It is complex and time consuming when the comprehensive dynamics of the MTDC power system are considered. Therefore, a part of the dynamics of the VSC and the remaining DC system (RDCS) is commonly excluded to simplify the stability analysis of the MTDC power system. We conducted some studies to investigate how the DC network affects DC voltage stability. For example, in [16], [17], the equivalent susceptance of the RDCS was ignored for simplification, and it was suggested that the negative equivalent conductance of the RDCS may lead to DC power oscillation. In [18], virtual damping analysis was applied to calculate the damping provided from each VSC to the DC voltage control loop. However, our previous studies have two limitations: (i) the imaginary part of the equivalent transfer function of VSCs in the DC voltage time scale was not considered, and (ii) the total impact of the RDCS including the comprehensive dynamics of DC lines was not investigated. The above omissions occurred because we agreed with the convention that ignoring parts of the dynamics of the MTDC power system would simplify the study and have a low impact on the conclusions.

However, we have become aware that these simplifications may lead to missing some instability risks or errors in the analyzed results. For example, the instability risk of the DC voltage oscillation cannot be identified if the DC voltage control loop of the VSC is ignored, and thus, the DC network is considered to connect to a constant DC voltage bus. Further, ignoring a part of the dynamics of the DC network and loads, or even representing them by resistances, can lead to errors in the conclusions because the actual dynamic responses of the DC network and loads are nonlinear instead of linear. Thus, it is meaningful to analyze DC voltage oscillation stability considering the comprehensive dynamics of the MTDC power system in a DC voltage time scale to reveal the stability mechanism of the DC voltage oscillation accurately.

In this study, comprehensive dynamics, including dynamics of the DC voltage control and DC transmission lines, of the MTDC power system in the DC voltage time scale are considered. Compared with the model that ignores dynamics of the DC voltage control or/and the DC network, the instability risk of the DC voltage oscillation can be accurately identified with the model established in this study, which fills the gaps in [19], [20]. Specifically, the MTDC power system with master slave control is firstly studied and then the proposed analysis method and obtained conclusions are applied to parts of the MTDC power systems using DC voltage droop control. The effect of dynamics of the VSC involved in DC voltage control and the dynamics of the RDCS on DC voltage oscillation stability are analyzed. It is indicated that the DC voltage oscillation loop is initially formed by the DC voltage control or DC voltage droop control of the VSC, and then, it is affected by the dynamics of the RDCS through two paths.

Subsequently, it is theoretically revealed how the dynamics of RDCS affect the stability of DC voltage oscillation through two paths, which is another major contribution of this study. It is demonstrated that: (i) the equivalent conductance of the RDCS is equal to an additional damping added to the DC voltage oscillation loop, and it directly changes the damping of the DC voltage oscillation. Consequently, increasing equivalent conductance of the RDCS can improve the stability of the DC voltage oscillation. Thus, equivalent conductance can be increased by optimizing the operating states of the MTDC power system to improve the stability of the DC voltage oscillation. (ii) the equivalent susceptance of the RDCS forms a mirrored subsystem of a feedforward subsystem that results in an open-loop modal resonance at the DC voltage time scale. Thus, the effect of the equivalent susceptance on DC voltage oscillation stability is always negative. This finding indicates that ignoring part of the dynamics of the RDCS can lead to missing some instability risks, which can result in misestimating the stability of the DC voltage oscillation.

Finally, considering that the traditional stable operating region of the MTDC power system is complex because many variables should be concerned and thereby resulting in high-dimension, a convenient method is proposed to determine the stable operating

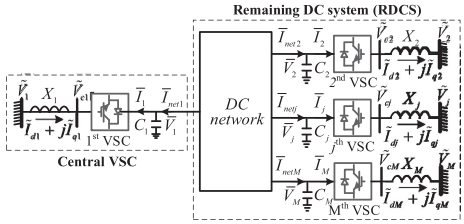

Fig. 1. Configuration of the MTDC power system with master slave control.

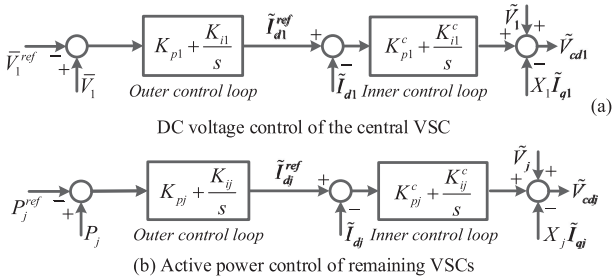

Fig. 2. Configuration of the control systems of M VSCs. (a) DC voltage control of the central VSC (b) Active power control of remaining VSCs.

region of the RDCS in a DC voltage time scale. The stable operating region is two-dimensional and the MTDC power system is stable as long as the equivalent conductance and susceptance of the RDCS are within the restrictions. It is meaningful for engineers as it is simple even if comprehensive dynamics of the MTDC power system are considered and can assist them to avoid the instability risk of the MTDC power system.

The contributions of this study are summarized as follows.

1) Dynamics in the DC voltage time scale of the MTDC power system were comprehensively considered, and thus can eliminate errors in investigating DC voltage oscillation stability compared with the model that ignores partial dynamics of the DC voltage control or/and the DC network.
2) The stability mechanism related to how comprehensive dynamics of the VSC involved in DC voltage control and those of the RDCS affect DC voltage oscillation stability was clarified accurately in all of the MTDC power systems using master slave control and parts of the MTDC power systems using DC voltage droop control.
3) A method of determining the stable operating region of the RDCS in the DC voltage time scale is proposed. The dimension is two and thus, is convenient for assisting engineers to avoid the instability risk of the MTDC power system even if much more dynamics are considered.

The rest of this manuscript is organized as follows: in Section II, an analysis is conducted based on the linearized model of the MTDC power system in a DC voltage time scale. In Section III, the stability mechanism of the DC voltage oscillation is clarified, and a numerical criterion for determining the effect of the RDCS is proposed. In Section IV, two case studies based on the SIMULINK platform are presented to demonstrate the accuracy of the stability mechanism of the DC voltage oscillation and the effectiveness of the proposed method. Finally, in Section V, the paper is summarized and the conclusions and contributions of the study are presented.

II. Linearized Model of MTDC Power System in DC Voltage Time Scale

A. Linearized Model of Each VSC Station Under Master Slave Control

The configuration of the MTDC power system connected with M VSCs is shown in Fig. 1. The type of the VSCs can be either two-level or three-level VSC. The analysis conducted in this study is applicable for the modular multilevel converter (MMC) if the control systems of the MMC are the same as those adopted in the study. Considering that this study focuses on small-signal DC voltage oscillation stability within an MTDC power system, VSCs are separately connected to M AC power systems represented by infinite buses [7], [8], [10]. Thus, the dynamics of the AC power systems are ignored, and the AC voltages at the point of common coupling (PCC) nodes are kept constant, i.e., $\Delta\tilde{V}_k = 0$ and $k = 1, 2, \ldots, \mathrm{M}$. Assuming that the direction of $\tilde{V}_k$ is along the d axis of the VSC d–q coordinate system (i.e., $\tilde{V}_{qk} = 0$, $\tilde{V}_{dk} = \tilde{V}_k$), we obtain

$$P_k = \tilde{V}_k \tilde{I}_{dk} = \bar{V}_k \bar{I}_k. \tag{1}$$

In Fig. 1, the central VSC controls the DC voltage stably, and the remaining VSCs (i.e., j^{th} VSC, $j = 2, 3, \ldots, \mathrm{M}$) control the active power. The configuration of the control system with M VSCs is shown in Fig. 2 [21]. For each VSC, the dynamic equation of the DC voltage is given by

$$C_k \frac{d\bar{V}_k}{dt} = \bar{I}_{netk} - \frac{P_k}{\bar{V}_k}. \tag{2}$$

The dynamic transfer function of the inner control loop can be represented by

$$\tilde{I}_{dk} = G_{idk}(s)\tilde{I}_{dk}^{ref}, \tag{3}$$

where $G_{idk}(s) = \frac{K_{pk}^c s + K_{ik}^c}{X_k \omega_0^{-1} s^2 + K_{pk}^c s + K_{ik}^c}$.

In (3), $G_{idk}(s)$ represents the dynamics of the inner current control loop. The inner current (approximately 10 ms) and the outer DC voltage control loops (around 100 ms) are in different time scales. This allows analyzing their dynamics separately [22], [23]. Thus, when the DC voltage oscillation is examined, the dynamics of current control can be ignored. It is considered that the current control can track their reference values instantaneously. Thus, $G_{idk}(s)$ is approximately equal to 1, and (3) can be simplified as $\tilde{I}_{dk} = \tilde{I}_{dk}^{ref}$.

According to Fig. 2(a), the transfer function of the outer control loop of the central VSC can be obtained as

$$\tilde{I}_{d1}^{ref} = \left(K_{p1} + K_{i1} s^{-1}\right)\left(\bar{V}_1 - \bar{V}_1^{ref}\right). \tag{4}$$

By linearizing (1), (2), and (4) at a steady state, the linearized model of the central VSC used to analyze the DC voltage oscillation is obtained as

$$s\mathbf{x}_1 = \mathbf{a}_1\mathbf{x}_1 + \mathbf{u}_1\Delta\bar{I}_{net1}, \Delta\bar{V}_1 = \mathbf{c}_1^m\mathbf{x}_1^m, \tag{5}$$

where $\mathbf{x}_1 = [\,\Delta\bar{V}_1\ \Delta\tilde{I}_{d1}\,]^T, \mathbf{u}_1 = [\,{C_1}^{-1}\ K_{p1}{C_1}^{-1}\,]^T, \mathbf{c}_1 = [\,1\ m0\,]$.

Furthermore, the transfer function of the DC voltage oscillation loop of the central VSC is given as

$$\Delta\bar{V}_1 = \mathbf{c}_1(s\mathbf{E} - \mathbf{a}_1)^{-1}\mathbf{u}_1\Delta\bar{I}_{net1} = \frac{K_4 s}{K_1 s^2 + K_2 s + K_3}\Delta\bar{I}_{net1}, \quad (6)$$

where $K_1 = C_1\bar{V}_1$, $K_2 = K_{p1}\tilde{V}_1 - \bar{I}_1$, $K_3 = K_{i1}\tilde{V}_1$, and $K_4 = \bar{V}_1$.

Similarly, the transfer function of the outer control loop of the slave VSC (j^{th} VSC, $j = 2, 3, \ldots, M$) can be obtained from Fig. 2(b) as

$$\Delta\tilde{I}_{dj} = \Delta\tilde{I}_{dj}^{ref} = \left(K_{pj} + \frac{K_{ij}}{s}\right)\Delta P_j. \quad (7)$$

Linearizing (1) and (2) at a steady state, yields

$$\Delta P_j = \tilde{V}_j\Delta\tilde{I}_{dj} + \tilde{I}_{dj}\Delta\tilde{V}_j \quad (8)$$

$$\Delta\bar{V}_j = \frac{\bar{V}_j}{sC_j\bar{V}_j - \bar{I}_j}\Delta\bar{I}_{netj} - \frac{1}{sC_j\bar{V}_j - \bar{I}_j}\Delta P_j \quad (9)$$

Substituting (7) into (8), it can be obtained that

$$\Delta P_j = \frac{\tilde{I}_{dj}s}{s - \tilde{V}_j\left(K_{pj}s + K_{ij}\right)}\Delta\tilde{V}_j \quad (10)$$

Equation (10) indicates that dynamics of the PI control of the slave VSCs are related to the AC active power and voltage, which can only be induced by the disturbance in the AC power systems. Focus of this study is the small-signal DC voltage oscillation stability within an MTDC power system. Hence, dynamics of the external AC power systems are ignored ($\Delta\tilde{V}_k = 0$) [7], [8], [10] such that $\Delta P_j = 0$. Subsequently, impact of dynamics of the PI control of the slave VSCs on the stability of the MTDC power system in the DC voltage time scale can be ignored. Thus, transfer function of the j^{th} VSC is obtained from (9) as

$$\Delta\bar{V}_j = \frac{-\bar{V}_j}{\bar{I}_j - sC_j\bar{V}_j}\Delta\bar{I}_{netj} = R_{ej}(s)\Delta\bar{I}_{netj}. \quad (11)$$

Equation (11) indicates that the active power-controlled VSC can be considered to be resistance if the dynamic response of the VSC is ignored (s = 0). However, this simplification can result in errors in the stability analysis of the DC voltage oscillation. Therefore, this study considers all the dynamics of the VSC in the DC voltage time scale for the accurate stability analysis of the DC voltage oscillation.

B. Linearized Model of Each VSC Station Under DC Voltage Droop Control

The configuration of the MTDC power system adopted DC voltage droop control is shown in Fig. 3. In this case, the central VSC is represented by *F* DC voltage droop controlled VSCs to control the DC voltage coordinately. Parameters of those VSCs are indicated by superscript '*d*'. The control configuration of the f^{th} DC voltage droop controlled VSC ($f = 1, 2, \ldots, F$) is shown in Fig. 4.

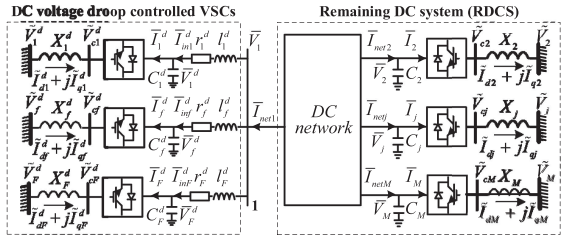

Fig. 3. Configuration of the MTDC power system with DC voltage droop control.

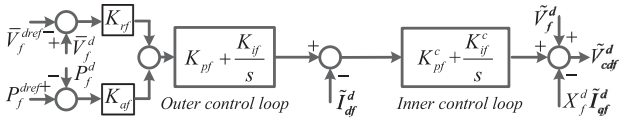

Fig. 4. Configuration of the DC voltage droop control.

Based on Fig. 4, the transfer function of the outer control loop of the f^{th} VSC ($f = 1, 2, \ldots, F$) is obtained as

$$\tilde{I}_{df}^d = \left(K_{pf} + \frac{K_{if}}{s}\right)\left(K_{rf}\left(\bar{V}_f^d - \bar{V}_f^{dref}\right) + K_{af}\left(P_f^{dref} - P_f^d\right)\right). \quad (12)$$

By linearizing (1), (2), and (12) at a steady-state operating point, following linearized model of the f^{th} VSC is obtained

$$\Delta\bar{V}_f^d = \frac{K_{f4}^d s + K_{f5}^d}{K_{f1}^d s^2 + K_{f2}^d s + K_{f3}^d}\Delta\bar{I}_{inf}^d, \quad (13)$$

where

$$K_{f1}^d = C_f^d\bar{V}_f^d + C_f^d\bar{V}_f^d\tilde{V}_f^d K_{pf}K_{af},$$
$$K_{f2}^d = \bar{I}_f^d + C_f^d\bar{V}_f^d\tilde{V}_f^d K_{if}K_{af} + \bar{I}_f^d\tilde{V}_f^d K_{pf}K_{af} - \tilde{V}_f^d K_{pf}K_{rf},$$
$$K_{f3}^d = \bar{I}_f^d\tilde{V}_f^d K_{if}K_{af} - \tilde{V}_f^d K_{if}K_{rf},$$
$$K_{f4}^d = \bar{V}_f^d + \bar{V}_f^d\tilde{V}_f^d K_{af}K_{pf},$$
$$K_{f5}^d = \bar{V}_f^d\tilde{V}_f^d K_{af}K_{if}.$$

Transfer function of *F* DC voltage droop controlled VSCs can be obtained from (13) as

$$\Delta\bar{\mathrm{V}}_1 = \left[\sum_{\mathrm{f}=1}^{\mathrm{F}}\frac{\mathrm{K_{f1}^d s^2 + K_{f2}^d s + K_{f3}^d}}{\mathrm{K_{f4}^d s + K_{f5}^d + \left(K_{f1}^d s^2 + K_{f2}^d s + K_{f3}^d\right)\left(r_f^d + sl_f^d\right)}}\right]^{-1} \times \Delta\bar{\mathrm{I}}_{net1} \quad (14)$$

In this study, the DC voltage stability of the MTDC power system using master slave control is mainly focused. And then, the proposed method and obtained conclusions are applied to a part of MTDC power systems with DC voltage droop control. Therefore, the form of (14) should be reconstructed so that can be similar to (6), which is the motivation of following derivations.

If transfer functions of *F* DC voltage droop controlled VSCs are same, the transfer function of each VSC can be written as

$$\Delta\bar{V}_f^d = \frac{K_{O4}^d s + K_{O5}^d}{K_{O1}^d s^2 + K_{O2}^d s + K_{O3}^d}\Delta\bar{I}_{inf}^d \tag{15}$$

where, $K_{O1} = K_{f1}^d$, $K_{O2} = K_{f2}^d$, $K_{O3} = K_{f3}^d$, $K_{O4} = K_{f4}^d$, $K_{O5} = K_{f5}^d$.

Under this condition, the transfer function of *F* DC voltage droop controlled VSCs is obtained from (14) and (15) as

$$\Delta\bar{V}_1 = \frac{K_{O4}^d s + K_{O5}^d + \left(K_{O1}^d s^2 + K_{O2}^d s + K_{O3}^d\right)\left(r_O^d + s l_O^d\right)}{K_1 s^2 + K_2 s + K_3} \times \Delta\bar{I}_{net1} \tag{16}$$

where, $K_1 = FK_{O1}^d$, $K_2 = FK_{O2}^d$, $K_3 = FK_{O3}^d$, $r_O^d = r_f^d$, $l_O^d = l_f^d$.

Equation (16) can be divided into

$$\Delta\bar{V}_1 = \left(H_0(s) + \Delta H_1(s)\right)\Delta\bar{I}_{net1} \tag{17}$$

where $H_0(s) = \frac{K_{O4}^d s}{K_1 s^2 + K_2 s + K_3}$,

$$\Delta H_1(s) = \frac{K_{O5}^d + \left(K_{O1}^d s^2 + K_{O2}^d s + K_{O3}^d\right)\left(r_O^d + s l_O^d\right)}{K_1 s^2 + K_2 s + K_3}.$$

In (17), $H_0(s)$ represents the part similar to (6), while $\Delta H_1(s)$ represents the part different from (6). Considering the operating states and parameters of VSCs are different, an additional part should be added to (17), yields

$$\Delta\bar{I}_{net1} = \left(H_0(s) + \Delta H_1(s) + \Delta H_2(s)\right)\Delta\bar{V}_1 \tag{18}$$

where, $\Delta H_2(s)$ represents the differences among VSCs, which can be obtained by subtracting (16) from (14). Normally, the VSCs are designed by a certain company, thus $\Delta H_2(s)$is small.

It can be seen from (18) that dynamics of the *F* DC voltage droop controlled VSCs can be represented by $H_0(s)$ and an equivalent series-connected resistance $r_F(s)$, where $r_F(s) = \Delta H_1(s) + \Delta H_2(s)$. In which, $r_F(s)$ can be classified into the DC network, so that the transfer function of the DC voltage oscillation loop of the DC voltage droop controlled VSCs is obtained as

$$\Delta\bar{V}_1 = \frac{K_4 s}{K_1 s^2 + K_2 s + K_3}\Delta\bar{I}_{net1} \tag{19}$$

where $K_4 = K_{O4}^d$.

It can be seen that the forms of (19) and (6) are similar, so the proposed methods are appliable for both of them.

C. Linearized Model When Dynamics of the DC Voltage Control are Simplified

If the DC voltage is considered to be controlled perfectly, the DC voltage is constant regardless of any effect of the RDCS. Thus, $\bar{V}_1 = 0$. With this assumption, the instability risk associated with the DC voltage oscillation is ignored. This may result in errors in the analyzed results.

If the dynamics of the DC voltage control loop are simplified by considering it as a first-order delay, it can have

$$\bar{V}_1 = \frac{1}{\tau s + 1}\bar{V}_1^{ref} \tag{20}$$

where τ is the time constant [24].

The reference of the DC voltage is a constant value of 1 p.u. Thus, $\Delta\bar{V}_1^{ref} = 0$. The dynamics of the DC voltage is obtained from (20) as

$$s\Delta\bar{V}_1 = \frac{1}{\tau}\left(\Delta\bar{V}_1^{ref} - \Delta\bar{V}_1\right) = -\frac{1}{\tau}\Delta\bar{V}_1 \tag{21}$$

It can be seen from (21) that the dynamics of the simplified first-order DC voltage control loop are determined by the pole $s = -\tau^{-1}$and not affected by the RDCS at all. Therefore, the instability risk associated with the DC voltage control may also be missed when a first-order simplified model is used to represent the DC voltage control loop.

D. State-Space Model of the MTDC Power System

Without loss of generality, using a high-order matrix $\mathbf{Y}_{DC}(s)$ representing a nonlinear relationship between the DC current output and the voltages at the ports of the DC network yields

$$\Delta\bar{\mathbf{I}}_{DC} = -\mathbf{Y}_{DC}(s)\Delta\bar{\mathbf{V}}_{DC}, \tag{22}$$

where $\Delta\bar{\mathbf{I}}_{DC} = [\Delta\bar{\mathbf{I}}_{net}^T, \mathbf{0}]^T$, $\Delta\bar{\mathbf{I}}_{net} = [\Delta\bar{I}_{net1} \cdots \Delta\bar{I}_{netM}]^T$, $\Delta\bar{\mathbf{V}}_{DC} = [\Delta\bar{\mathbf{V}}_{1-M}^T, \Delta\bar{\mathbf{V}}_{(M+1)-N}^T]^T$, $\Delta\bar{\mathbf{V}}_{1-M} = [\Delta\bar{V}_1 \cdots \Delta\bar{V}_M]^T$, and $\Delta\bar{\mathbf{V}}_{(M+1)-N} = [\Delta\bar{V}_{M+1} \cdots \Delta\bar{V}_N]^T$.

Eliminating zero elements in $\Delta\bar{\mathbf{I}}_{DC}$, yields

$$\begin{aligned}\Delta\bar{\mathbf{I}}_{net} &= -\left(\mathbf{Y}_{11}(s) - \mathbf{Y}_{12}(s)\mathbf{Y}_{22}(s)^{-1}\mathbf{Y}_{21}(s)\right)\\ &= -\mathbf{Y}_{net}(s)\Delta\bar{\mathbf{V}}_{1-M},\end{aligned} \tag{23}$$

where $\mathbf{Y}_{11}(s)$ comprises the 1st to Mth rows and the columns of $\mathbf{Y}_{DC}(s)$;$\mathbf{Y}_{12}(s)$ comprises the 1st to Mth rows and the Mth to Nth columns of $\mathbf{Y}_{DC}(s)$; $\mathbf{Y}_{21}(s)$ comprises the Mth to Nth rows and 1st to Mth columns of $\mathbf{Y}_{DC}(s)$; and $\mathbf{Y}_{22}(s)$ denotes the entry at the intersection of the Mth to Nth rows and columns of $\mathbf{Y}_{DC}(s)$.

From (11), dynamics of the active power-controlled VSCs can be obtained as

$$\begin{bmatrix}\Delta\bar{V}_2\\ \vdots\\ \Delta\bar{V}_M\end{bmatrix} = \begin{bmatrix}R_{e2}(s) & & \\ & \ddots & \\ & & R_{eM}(s)\end{bmatrix} = \mathbf{R}(s)\begin{bmatrix}\Delta\bar{I}_{net2}\\ \vdots\\ \Delta\bar{I}_{netM}\end{bmatrix}. \tag{24}$$

Substituting (24) into (23), yields

$$\Delta\bar{I}_{net1} = -y_{net}(s)\Delta\bar{V}_1, \tag{25}$$

where $y_{net}(s) = y_{11}(s) - \mathbf{y}_{12}(s)(\mathbf{R}(s)^{-1} + \mathbf{y}_{22}(s))^{-1}\mathbf{y}_{21}(s) + y_F(s)$.

$y_{11}(s)$ comprises the 1st row and column of $\mathbf{Y}_{net}(s)$;$\mathbf{y}_{12}(s)$ comprises the 1st row and the 2nd to Mth columns of $\mathbf{Y}_{net}(s)$; $\mathbf{y}_{21}(s)$ comprises the 1st to Mth rows and 1st column of $\mathbf{Y}_{net}(s)$; and $\mathbf{y}_{22}(s)$ denotes the entry at the intersection of the 2nd to Mth rows and columns of $\mathbf{Y}_{net}(s)$.

It can be seen from (25) that when full dynamics of the DC network are considered, $y_{net}(s)$ is composed of multiple high-order equations in 's' domain instead of a resistive matrix, which is complex for stability analysis. Considering the weak-damping DC voltage oscillation mode, denoted as $\lambda_d = -\varepsilon_d + j\omega_d$, is mainly focused in stability analysis, so that $\varepsilon_d \ll \omega_d$. Under these conditions, (25) can be replaced by

$$y_{net}(s) = y_{net}(\lambda_d) \approx y_{net}(j\omega_d) = y_{net}, \tag{26}$$

where $s = j\omega_d$ is used to approximately replace $s = \lambda_d$.

Here, y_{net} is a complex number. The physical meaning of y_{net} is the equivalent admittance of the RDCS in the DC voltage time scale. But, if the condition $y_{net}(\lambda_d) \approx y_{net}(j\omega_d)$ is not met, the replacement $s = j\omega_d$ should be banned, and an accurate replacement of λ_d should be reselected.

Expressing (26) in the real matrix form,

$$\begin{bmatrix} \Delta\bar{I}_{net1} \\ \Delta\bar{I}'_{net1} \end{bmatrix} = -\begin{bmatrix} g_{net} & b_{net} \\ -b_{net} & g_{net} \end{bmatrix} \begin{bmatrix} \Delta\bar{V}_1 \\ \Delta\bar{V}'_1 \end{bmatrix} \tag{27}$$

where g_{net} and b_{net} are the real and imaginary parts of y_{net}, respectively.

The physical meaning of g_{net} and b_{net} is the equivalent conductance and susceptance of the RDCS in the DC voltage time scale, respectively. Substituting (27) in (6), the state-space model of the MTDC power system considering all dynamics in the DC voltage time scale when utilizing master slave is derived as

$$s\mathbf{X}_F = \mathbf{A}_F\mathbf{X}_F, \tag{28}$$

where $\mathbf{X}_F = \begin{bmatrix} \mathbf{x}_1 \\ \mathbf{x}_1 \end{bmatrix}$, $\mathbf{A}_F = \begin{bmatrix} \mathbf{a}_1 & \mathbf{0} \\ \mathbf{0} & \mathbf{a}_1 \end{bmatrix} - \begin{bmatrix} \mathbf{u}_1 g_{net}\mathbf{c}_1 & \mathbf{u}_1 b_{net}\mathbf{c}_1 \\ -\mathbf{u}_1 b_{net}\mathbf{c}_1 & \mathbf{u}_1 g_{net}\mathbf{c}_1 \end{bmatrix}$.

If the MTDC power system with DC voltage droop control shown in Fig. 3 is focused. The transfer function of the VSC in (6) should be replaced by that in (19). $r_F(s)$ is classified into the DC network, so the transfer function of the DC network should be modified from (25) to be

$$\Delta\bar{I}_{net1} = -y_{net}(s)\Delta\bar{V}_1, \tag{29}$$

where

$$y_{net}(s) = \left[\left[y_{11}(s) - \mathbf{y}_{12}(s)\left(\mathbf{R}(s)^{-1} + \mathbf{y}_{22}(s)\right)^{-1}\mathbf{y}_{21}(s)\right]^{-1} + r_F(s)\right]^{-1}$$

Based on (29) and (19), model of the MTDC power system with DC voltage droop control can be obtained using similar derivations in (26) and (27).

In (26), the replacement $s = j\omega_d$ is used to simplify high-order dynamics of the RDCS. Doing so, high-order equations in $y_{net}(s)$ are represented by complex numbers. This method is usually used in analyzing damping torque of AC generators or VSCs [18]. It should be noted that the replacement may induce errors in calculated results since $\varepsilon_d \neq 0$. However, considering the weak-damping DC voltage oscillation mode is mainly focused in the stability analysis, so that $\varepsilon_d \ll \omega_d$. In this case, using $s = j\omega_d$ replaces $s = \lambda_d$ can approximately evaluate the effects of the RDCS in DC voltage time scale and significantly reduce the high-order dynamics of the RDCS. In determining critical stability of the DC voltage oscillation, using $s = j\omega_d$ does not affect the analyzed results of the critical DC voltage oscillation stability since $\lambda_d = j\omega_d$ under this condition. If the condition of (26) is invalid, the replacement $s = j\omega_d$ should be banned, and an accurate replacement of λ_d should be selected.

Regarding a specific MTDC power system, the frequency can be measured and determined by Fast Fourier Transform (FFT) analysis method. If the MTDC power system using DC voltage droop control has multiple oscillation modes in range of the DC voltage oscillation frequency, only the DC voltage oscillation mode with the worst-damping should be concerned and its frequency needs to be detected. It is unnecessary to determine all frequencies. If there are two oscillation modes with similar oscillation frequency, and the damping of them is significantly different, the oscillation frequency of the weak-damping oscillation mode can be measured by analyzing the data at end of the curve. If there are two oscillation modes with similar oscillation frequency and damping, these frequencies can be identified by increasing the sampling frequency, and the length of the sampled points. If we cannot obtain the accurate frequency of the weak-damping oscillation mode, such as the MTDC power system is in planning stage, we can determine frequency range of the frequency, the MTDC power system is stable as long as it is stable at each frequency point in the range.

It can be seen that the form of (19) is similar to that of (6), so that the proposed analysis method and obtained conclusions of the MTDC power system using master slave control can be applied to analyze DC voltage stability of this DC voltage droop controlled MTDC power system. Obviously, regarding the other MTDC power systems that cannot be written as a single-input and single-output transfer function as shown in (19), the proposed analysis method and obtained conclusions are invalid. So, the reason for deriving (15)–(19) is to obtain the single-input and single-output transfer function of multiple DC voltage droop controlled VSCs. In actual, many topologies of the DC voltage droop controlled MTDC power system can satisfy above conditions, but the parallel connection of VSCs is usual and easy for readers to understand how to apply the proposed analysis method to analyze the DC voltage stability of a DC voltage droop controlled MTDC power system.

The phenomenon of multiple DC voltage oscillation modes was found in [16]. However, the condition of this phenomenon is unusual because it needs an extremely long transmission line, about 2000 km as reported in [16]. Excluding [16], any other papers that reported this phenomenon were not found. General conclusion is that the MTDC power system with DC voltage droop control has only one DC voltage oscillation mode [25], [26]. Therefore, this study mainly focuses on DC voltage stability mechanism of the MTDC power system using master slave control, and then examines the effectiveness of the proposed analysis method in a DC voltage droop controlled MTDC power system. The latter can be written in the form of a single-input and single-output and has only one DC voltage oscillation mode.

E. Transfer Function Model of the MTDC Power System

Fig. 5 shows the block diagram model of the MTDC power system that considers the dynamics in the DC voltage time scale.

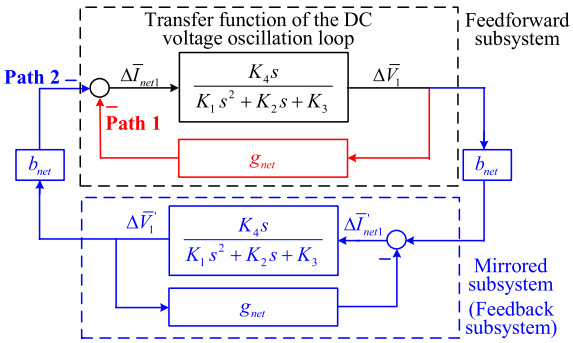

Fig. 5. Transfer block model of the MTDC power system.

The transfer function of the DC voltage oscillation loop of the VSC is the part in dark color. Values of various coefficients are calculated by using (6) and (19) for the case of either master slave control or DC voltage droop control. From Fig. 5, it can be seen that the DC voltage oscillation loop is affected by the dynamics in two feedback paths. The effect of feedback path 1 is caused by the equivalent conductance of the RDCS. This path is expressed as

$$\begin{aligned}\Delta\bar{V}_1 &= \frac{sK_4}{K_1s^2+K_2s+K_3}\Delta\bar{I}_{net1}\\ &= \frac{sK_4}{K_1s^2+K_2s+K_3}\left(-g_{net}\Delta\bar{V}_1-\Delta\bar{V}_1'b_{net}\right)\\ &= -\frac{sb_{net}K_4}{K_1s^2+(K_2+K_4g_{net})s+K_3}\Delta\bar{V}_1' = -\frac{sb_{net}K_4}{F_R(s)}\Delta\bar{V}_1'\end{aligned} \tag{30}$$

The equivalent susceptance forms a mirrored subsystem of the feedback subsystem. The mirrored subsystem affects the DC voltage oscillation loop through path 2. Similar to (30), the transfer function of the mirrored subsystem is

$$\begin{aligned}\Delta\bar{V}_1' &= \frac{sK_4}{K_1s^2+K_2s+K_3}\Delta\bar{I}_{net1}'\\ &= \frac{sK_4}{K_1s^2+K_2s+K_3}\left(\Delta\bar{V}_1b_{net}-g_{net}\Delta\bar{V}_1'\right)\\ &= \frac{sb_{net}K_4}{K_1s^2+(K_2+K_4g_{net})s+K_3}\Delta\bar{V}_1 = \frac{sb_{net}K_4}{F_R(s)}\Delta\bar{V}_1\end{aligned} \tag{31}$$

Substituting (31) in (30), the characteristic equation of the MTDC power system is obtained as

$$-\frac{sb_{net}K_4}{F_R(s)}\frac{sb_{net}K_4}{F_R(s)} = 1. \tag{32}$$

Equation (32) is equivalent to

$$F_R(s)^2 + s^2{K_4}^2b_{net}^2 = 0 \tag{33}$$

Based on (28) and (33), the DC voltage oscillation mode can be calculated to evaluate the DC voltage oscillation stability of the MTDC power system.

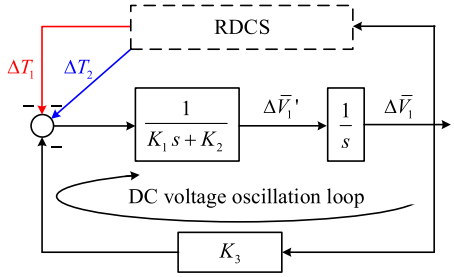

Fig. 6. DC voltage oscillation loop of the VSC involved in DC voltage control.

III. Stability Analysis of the DC Voltage Oscillation

A. Stability Mechanism of the DC Voltage Oscillation

Fig. 6 shows the DC voltage oscillation loop of the VSC involved in DC voltage control where ΔT_1 and ΔT_2 represent the effect of the RDCS through paths 1 and 2, respectively. First, the effect of the RDCS is not considered, and the characteristic equation of the DC voltage oscillation loop is obtained as

$$\left(K_1s^2+K_2s+K_3\right)\Delta\bar{V}_1 = 0. \tag{34}$$

The solution for (34) can be written as

$$\bar{V}_1(t) = ae^{-\frac{K_2}{2K_1}t}\cos(\omega_d t) + b, \tag{35}$$

where $\omega_d = \frac{1}{2}\sqrt{\left(\frac{K_2}{K_1}\right)^2 - \frac{4K_3}{K_1}}$ and $D_d = \frac{K_2}{2K_1}$ denote the frequency and damping of the DC voltage oscillation, respectively.

From (35), it can be concluded that D_d determines whether the DC voltage oscillation is convergent or divergent. Therefore, the DC voltage oscillation is stable only if $K_2 > 0$, which is satisfied because the VSC involved in DC voltage control is self-stable in general.

If the equivalent conductance of RDCS is considered, the characteristic equation of the DC voltage oscillation loop can be rewritten as

$$\left(K_1s^2+K_2s+K_3\right)\Delta\bar{V}_1 - \Delta T_1 = 0. \tag{36}$$

The input signal ΔT_1 can be derived as

$$\Delta T_1 = -sg_{net}K_4\Delta\bar{V}_1. \tag{37}$$

Substituting (37) in (36), the characteristic equation of the DC voltage oscillation loop considering the effect of the equivalent conductance is obtained as

$$\left(K_1s^2+(K_2+g_{net}K_4)s+K_3\right)\Delta\bar{V}_1 = 0. \tag{38}$$

Equation (38) indicates that the damping of the DC voltage oscillation changes to $(K_2+g_{net}K_4)/(2K_1)$, whereas the frequency of the DC voltage oscillation remains unchanged. This indicates that the equivalent conductance of the RDCS does not affect the frequency of the DC voltage oscillation. Further, this is equal to an additional damping to the DC voltage oscillation loop. The damping of the DC voltage oscillation reduces if $g_{net} < 0$, and it improves if $g_{net} > 0$. This is consistent with the traditional cognition that negative resistance can decrease the stability of the MTDC power system.

The equivalent susceptance of the RDCS forms a mirrored subsystem and connects two identical subsystems, which leads to an open-loop modal resonance. The open-loop modal resonance poses a threat to the stability of the system because it can induce strong mutual exclusion phenomenon between the open-loop oscillation modes of the connected subsystems [27], [28], which is explained in detail in Appendix A. Under this condition of open-loop modal resonance, ΔT_2 increases significantly and negatively affects the DC voltage oscillation. The detailed analysis is presented below.

Equation (33) is divided as

$$(F_R(s) + sK_4 b_{net} j)\,(F_R(s) - sK_4 b_{net} j) = 0. \tag{39}$$

At frequency ω_d, the solutions of (39) are approximately equal to two sub-equations as

$$\begin{aligned}&(K_1 + K_4 b_{net} {\omega_d}^{-1}) s^2 + (K_2 + K_4 g_{net}) s + K_3 = 0\\ &(K_1 - K_4 b_{net} {\omega_d}^{-1}) s^2 + (K_2 + K_4 g_{net}) s + K_3 = 0.\end{aligned} \tag{40}$$

The damping of the worst DC voltage oscillation mode is calculated from (40) as

$$D_d = \frac{K_2 + K_4 g_{net}}{2\,(K_1 + K_4\,|b_{net}|\,{\omega_d}^{-1})}. \tag{41}$$

Equation (41) indicates that the effect of the equivalent susception on DC voltage oscillation is always negative owing to the open-loop modal resonance [27], [28]. Moreover, the effect on DC voltage oscillation is related only to the amplitude of equivalent susception regardless of whether it is reactive or capacitive. Further, $|b_{net}|$ represents the strength of the connection between the feedforward and mirrored subsystems. The increase in $|b_{net}|$ can lead to stronger open-loop modal resonance and amplify the interaction between two interconnected subsystems. Consequently, the damping of the DC voltage oscillation becomes worse, which further reduces the stability of the DC voltage oscillation.

Therefore, the stability mechanism of the DC voltage oscillation is clarified. The DC voltage oscillation loop is initially formed by the DC voltage control of the VSC involved in DC voltage control, and it is affected by the dynamics of the RDCS. The equivalent conductance of the RDCS is equal to an additional damping to the DC voltage oscillation loop, and it directly changes the damping of the DC voltage oscillation. The equivalent susceptance of the RDCS forms a mirrored subsystem that results in an open-loop modal resonance at the DC voltage time scale. The effect of equivalent susceptance on DC voltage oscillation stability is always negative, and excluding this may lead to missing some instability risks, which can cause the mis-determination of the stability of DC voltage oscillation.

B. Effect of the RDCS on Stability of the DC Voltage Oscillation

The effect of changing the equivalent conductance and susceptance on the damping of the DC voltage oscillation is different. The variation in the damping of the DC voltage oscillation when the per equivalent conductance changes is

$$\frac{\Delta D_d}{\Delta g_{net}} = \frac{K_4}{2\,(K_1 + K_4\,|b_{net}|\,\omega_d{}^{-1})} > 0. \tag{42}$$

Changing the equivalent susceptance yields

$$\frac{\Delta D_d}{\Delta\,|b_{net}|} = -\frac{(K_2 + K_4 g_{net})\,K_4 \omega_d{}^{-1}}{2(K_1 + K_4\,|b_{net}|\,\omega_d{}^{-1})^2} < 0. \tag{43}$$

Equations (42) and (43) indicate that the effect of increasing per equivalent conductance and susceptance on the damping of the DC voltage oscillation decreases if $|b_{net}|$ increases, which is a nonlinear relationship. A stable MTDC power system has $K_2 + K_4 g_{net} > 0$, and thus increasing $\Delta g_{net}$and $\Delta|b_{net}|$ can separately improve and reduce the damping of the DC voltage oscillation.

The positive effect of per Δg_{net} is offset by the negative effect of per $\Delta|b_{net}|$, and this reduces the stability of the DC voltage oscillation if the following condition is satisfied:

$$g_{net} {K_4}^2 + K_2 K_4 > K_4\,|b_{net}| + K_1 \omega_d. \tag{44}$$

Conversely, the positive impact of per Δg_{net} is larger, and the damping of the DC voltage oscillation is increased. The collective effect of equivalent conductance and susceptance on the damping of the DC voltage oscillation is analyzed below.

If g_{net} is negative, the damping of the DC voltage oscillation is reduced because the effect of the equivalent conductance and susceptance are both negative. If g_{net} is positive, the effect of the equivalent conductance is positive, and that of the equivalent susceptance is negative. Therefore, these two effects need to be compared to determine the total effect of the RDCS.

The effect of the RDCS is positive if

$$g_{net} > \frac{K_2\,|b_{net}|}{K_1 \omega_d}. \tag{45}$$

Conversely, the effect of the RDCS is negative, and the stability of the DC voltage oscillation is reduced. In the worst case, if $K_2 + K_4 g_{net} < 0$, the DC voltage oscillation loses stability. The steps to determine and further improve the effect of the RDCS on the stability of the DC voltage oscillation are listed below:

1) Identify the DC voltage oscillation loop formed by VSCs either with DC voltage control or DC voltage droop control.
2) Calculate the equivalent conductance and susceptance of the RDCS in the frequency of the DC voltage oscillation, and the effect of the RDCS using Equation (45). If the effect is positive, no additional restrictions are needed; otherwise, proceed to Step 3 to reduce the negative effects.
3) Conduct an in-depth analysis using Equations (42)–(45), to determine whether equivalent conductance or susceptance is the primary reason for reducing the damping of the DC voltage oscillation. Then, use some methods to increase g_{net} and/or decrease $|b_{net}|$. Two alternative methods can be considered to improve the damping of the DC voltage oscillation: i) install additional damping controller in the MTDC power system. The installation can be either on the VSCs in the RDCS to reduce the

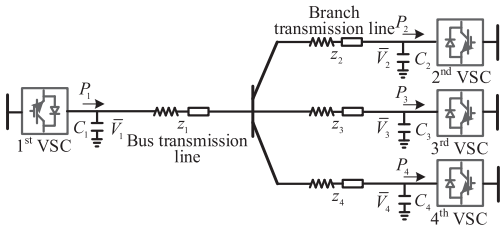

Fig. 7. Four-terminal MTDC power system.

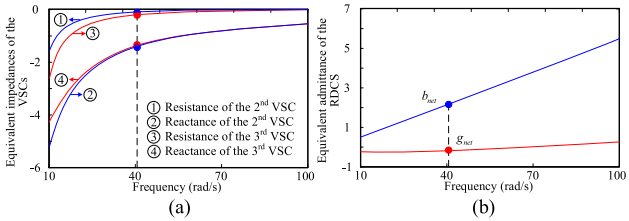

Fig. 8. Frequency sweeping results. (a) Impedances of the active power controlled VSCs, and (b) Equivalent conductance and susceptance of the RDCS.

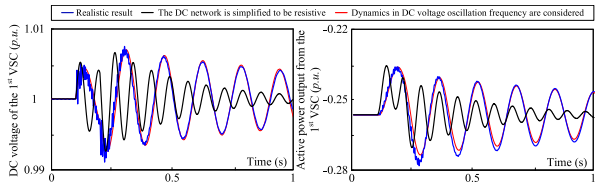

Fig. 9. Nonlinear simulation results (DC voltage of and active power output from the 1st VSC).

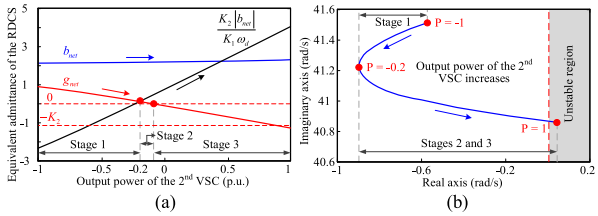

Fig. 10. Trajectories when the output power of the 2nd VSC increases from -1 to 1 p.u. (a) Trajectories of g_{net}, b_{net}, and (b) the DC voltage oscillation mode.

negative effect provided by the RDCS or on the VSCs with the DC voltage control such that the MTDC power system has a higher ability to withstand the negative effect of the RDCS. This method is suitable for the case that the MTDC power system connects with heavy loads. ii) limit the output power of the VSCs coordinately in the stable region of the RDCS. This method is suitable for the case that the margin of the output power of the MTDC power system is large and can be adjusted.

IV. Case Studies

The configuration of an exemplification MTDC power system that adopts a master–slave control is shown in Fig. 7. The configuration is radial and includes four VSC stations. The 1st VSC adopts DC voltage control; the remaining VSCs adopt active power control. The details of the parameters and loading conditions are provided in Table 1 in Appendix A [29]–[31].

A. Calculation and Validation of the Equivalent Conductance and Susceptance of the RDCS

Initially, the active power outputs from the slave VSCs are 0.05, 0.1, and 0.1 p.u. The frequency of the DC voltage oscillation $\omega_d = 41.13$ rad/s. The frequency sweeping results of the active power-controlled VSCs are shown in Fig. 8(a) and that of the RDCS are shown in Fig. 8(b).

Fig. 8(b) indicates that b_{net} significantly increases with an increase in the frequency of the DC voltage oscillation; this indicates that the equivalent susceptance of the RDCS affects the stability of the DC voltage oscillation more at higher oscillation frequencies. At the DC voltage oscillation frequency, g_{net} is negative owing to the negative impedances of the VSCs. Therefore, the collective effect of the RDCS on the stability of the DC voltage oscillation is negative in this case.

At the DC voltage oscillation frequency, $g_{net} = -0.1764$, $b_{net} = 2.193$, and the calculated results of the central VSC are $K_1 = 6.59$, $K_2 = 0.3$, and $K_3 = 0.318$. Thus, the damping of the DC voltage oscillation is predicted using Equation (41) as

$$D_d = -\frac{K_2 + \bar{V}_1 g_{net}}{2\left(K_1 + \bar{V}_1 |b_{net}| \omega_d{}^{-1}\right)} \times \omega_0 = -1.40(rad/s). \tag{46}$$

Damping of the DC voltage oscillation dominated by the central VSC is -8.14 rad/s when the impact of the RDCS is not considered. However, when the impact of the dynamics of the RDCS is considered, the damping of the DC voltage oscillation is -1.40 rad/s as indicated by (46). Hence, the dynamics of the RDCS affect the damping of DC voltage oscillation negatively. In this case, ignoring the impact of the dynamics of the RDCS may result in wrong assessment of the instability risk associated with the DC voltage oscillation. If the DC network is considered to be resistive and the equivalent susceptance of the RDCS is zero, damping of the DC voltage oscillation is calculated to be -3.53 rad/s.

To further confirm this result, the standard SIMULINK model is established, and the 1980-Hz 3-level 3-phase VSC from the SimPowerSystems-Toolbox is adopted [31]. The VSC control system uses two control loops: an external control loop that regulates DC voltage and an internal control loop that regulates grid currents. The voltage outputs of the current controller are converted to three modulating signals used by the PWM generator. The nonlinear simulation results are shown in Fig. 9 for the case when the AC voltage of the 2nd VSC drops to 5% at 0.1 s and then recovers at 0.2 s. From the simulation results presented in Fig. 9, the damping of the DC voltage oscillation is measured using Prony's analysis to be -0.87, which is close to the computational result given in (46). This confirms that considering comprehensive dynamics of the RDCS in the DC voltage time scale can effectively minimize the computational error.

B. Effect of Power Flow on DC Voltage Oscillation Stability

Fig. 10 shows the trajectories of g_{net}, b_{net}, and the DC voltage oscillation mode obtained by increasing the output power of the

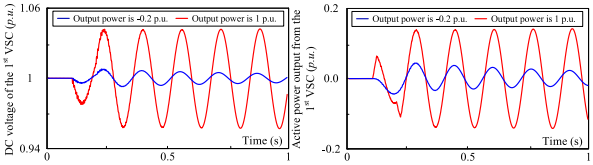

Fig. 11. Nonlinear simulation results when the output power of the 2nd VSC increases (DC voltage of and active power output from the 1st VSC).

2nd VSC from -1.0 p.u. to 1.0 p.u.; g_{net} decreases with an increase in the output power of the 2nd VSC. Further, there are three stages during power flow reversal.

Stage 1: $g_{net} > 0$ and $b_{net} > 0$. They separately cause positive and negative effects on the stability of the DC voltage oscillation. Considering $g_{net} > K_2|b_{net}|(K_1\omega_d)^{-1}$, the positive effect of g_{net} is larger than the negative effect of b_{net}, which improves the damping of the DC voltage oscillation mode.

Stage 2: $g_{net} > 0$, $b_{net} > 0$, and $g_{net} < K_2|b_{net}|(K_1\omega)^{-1}$. The positive effect of g_{net} is less than the negative effect of b_{net}, which decreases the damping of the DC voltage oscillation mode.

Stage 3: $g_{net} < 0$ and $b_{net} > 0$. Their effect on the stability of the DC voltage oscillation is negative, which decreases the damping of the DC voltage oscillation mode. In the worst-case scenario, $g_{net} < -K_2$, where the DC voltage oscillation becomes unstable.

In each stage, b_{net} rarely changes, which indicates that the stability of the DC voltage oscillation is affected by the equivalent conductance of the RDCS when the power flow reverses. Further, the effect of g_{net} on the damping of the DC voltage oscillation is nonlinear, as indicated in stages 1 and 2; this is because the effect of b_{net} is additionally considered. However, if we consider the RDCS as resistance and exclude the effect of b_{net}, the effect of g_{net} on the damping of the DC voltage oscillation is approximately linear, which is an incorrect conclusion when the system operates in stage 1. Thus, it is necessary to consider the dynamics of the RDCS comprehensively, and ignoring a part of it, such as b_{net}, can lead to errors in the conclusions.

The nonlinear simulation results when the output powers of the 2nd VSC are -0.2 and 1.0 p.u. are illustrated in Fig. 11. Increasing the output power without limitations will lead to the instability of the MTDC power system.

C. Impact of Length of the Transmission Line on DC Voltage Oscillation Stability

At the steady state, the active power output from the slave VSCs is 0.05, 0.1, and 0.1 p.u. Fig. 12 shows the trajectories of g_{net}, b_{net}, and the DC voltage oscillation mode when the branch transmission line of the 2nd VSC is increased from 10 to 510 km. As shown in Fig. 12, g_{net} decreases and b_{net} increases with an increase in the length of the branch transmission line, which indicates that the effect of the RDCS is negative. The increase in the branch transmission line leads to a DC voltage oscillation mode that moves to the right side of the complex plane. In the worst-case scenario, $g_{net} < -K_2$, the DC voltage oscillation becomes unstable.

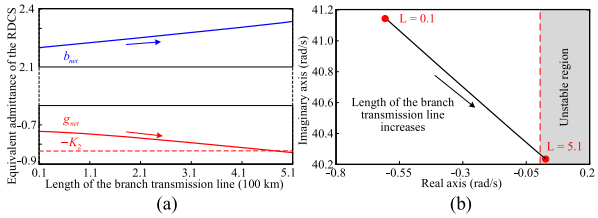

Fig. 12. Trajectories when length of the branch transmission line of the 2nd VSC increases. (a) Trajectories of g_{net}, b_{net}, and (b) the DC voltage oscillation mode.

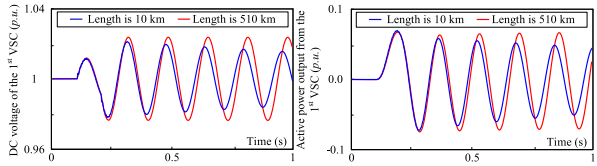

Fig. 13. Nonlinear simulation results when branch transmission line of the 2nd VSC increases. (DC voltage of and active power output from the 1st VSC).

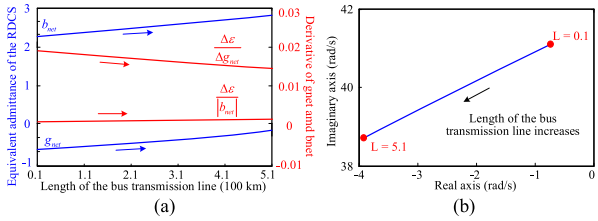

Fig. 14. Trajectories when the length of the bus transmission line of the RDCS increases. (a) Trajectories of g_{net}, b_{net}, and (b) the DC voltage oscillation mode.

In this case, excluding b_{net} does not change the conclusion that increasing the length of the branch line decreases the stability of the DC voltage oscillation; however, it may result in misestimating the instability risk of the DC voltage oscillation. As indicated in Fig. 12, the system loses stability when the length of the branch transmission line is 510 km. However, if the negative effect of b_{net} is not considered, this instability risk is missed, and it can lead to the incorrect determination of DC voltage oscillation stability.

The nonlinear simulation results are illustrated in Fig. 13. Herein, the lengths of the branch transmission lines of the 2nd VSC are 10 km and 510 km.

Fig. 14 shows the trajectories of g_{net}, b_{net}, and the DC voltage oscillation mode while increasing the length of the bus transmission line of the RDCS from 10 to 510 km. g_{net} and b_{net} consistently increase with an increase in the length of the bus transmission line. In this case, we cannot determine the collective effect of the RDCS directly because g_{net} and b_{net} have opposite effects on the stability of the DC voltage oscillation. Thus, the derivatives of the DC voltage oscillation damping with respect to g_{net} and b_{net} are indicated by red lines in Fig. 14; changing the Δg_{net} can result in a higher number of positive effects on DC voltage oscillation damping such that the collective effect of the RDCS is positive.

The nonlinear simulation results are illustrated in Fig. 15. Herein, the lengths of the bus transmission lines of the RDCS are 10 km and 510 km. Comparing the results shown in Figs. 14 and 15 indicates that the effect of increasing the transmission

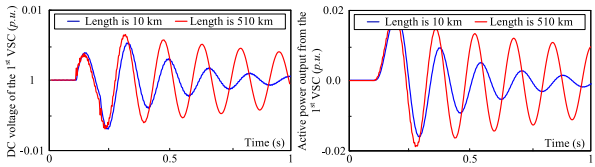

Fig. 15. Nonlinear simulation results when the bus transmission line of the RDCS increases. (DC voltage of and active power output from the 1st VSC).

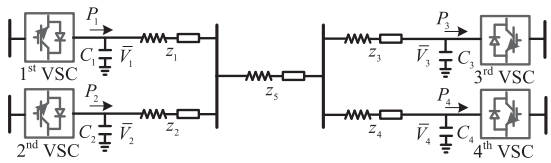

Fig. 16. Four-terminal MTDC power system.

line length on the stability of the DC voltage oscillation differs because g_{net} and b_{net} are changed differently.

D. Stability Analysis of the MTDC Power System With DC Voltage Droop Control

The configuration of an exemplification MTDC power system that adopts a DC voltage droop control is shown in Fig. 16. The 1st and 2nd VSCs adopt DC voltage droop control, and the remaining VSCs adopt active power control.

Initially, the active power outputs from the 3rd and 4th VSCs are 0.74 p.u. and 0.84 p.u., respectively. The frequency of the DC voltage oscillation is $\omega_d = 54.94$ rad/s. At the DC voltage oscillation frequency, $g_{net} = -0.8208$, $b_{net} = 1.2959$, and the calculated results of the DC voltage oscillation loop are $K_1 = 6.59$, $K_2 = 0.943$, $K_3 = 0.336$, and $K_4 = 1$. Thus, the damping of the DC voltage oscillation is predicted as

$$D_d = -\frac{K_2 + K_4 g_{net}}{2\left(K_1 + K_4 \left|b_{net}\right| \omega_d{}^{-1}\right)} \times \omega_0 = -1.48(rad/s). \tag{47}$$

The damping of the DC voltage oscillation dominated by the DC voltage droop controlled VSCs is -26.97 rad/s when the impact of the RDCS is not considered. However, as negatively affected by dynamics of the RDCS, the damping of the DC voltage oscillation is reduced to be -1.48 rad/s. It demonstrates that the dynamics of the RDCS reduce the stability of the DC voltage oscillation. In this case, neglection of the dynamics may result in errors in DC voltage oscillation stability. If the DC network is considered to be resistive and thus, equivalent susceptance of the RDCS equals to zero, damping of the DC voltage oscillation is calculated as -3.51 rad/s. The realistic damping of the DC voltage oscillation is calculated by full-order model as -1.71, which is closer to the result of (47).

As the output power of the 3rd VSC and the 4th VSC increases to 0.95 p.u. and 1.05 p.u., respectively, the damping of the DC voltage oscillation is calculated as 0.35 rad/s. It indicates that the DC voltage oscillation occurs since the damping of the DC voltage oscillation is negative. The realistic damping of the DC voltage oscillation is calculated by full-order model as 0.41, which demonstrates the analyzed results can determine DC voltage oscillation stability accurately.

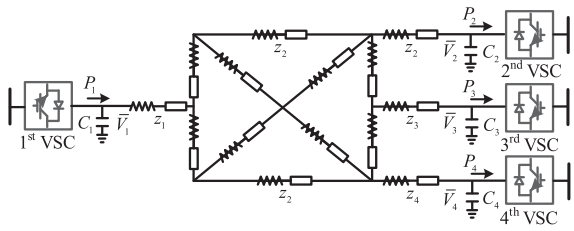

Fig. 17. An example complex VSC-MTDC power system.

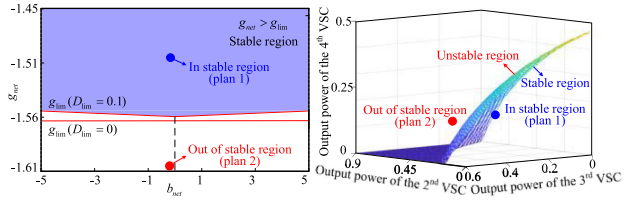

Fig. 18. Stable regions of the RDCS. (a) Stable region of the RDCS, and (b) traditional stable region of the operating states of the VSCs.

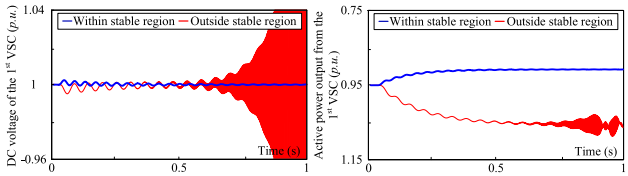

Fig. 19. Nonlinear simulation results of two cases within and outside of the stable regions. (DC voltage of and active power output from the 1st VSC).

E. Stable Region of the RDCS of the Complex MTDC System

The configuration of an example complex MTDC power system that adopts the master–slave control is shown in Fig. 17. The 1st VSC adopts the DC voltage control. The remaining VSCs use the active power control. In this case, the margin of the output power of the MTDC power system is large and can be adjusted. Thus, in the two-dimension stable region of the RDCS, the output power of the VSCs can be adjusted to improve the system stability associated with the DC voltage oscillation, as demonstrated as follows.

In Fig. 18(a), $g_{\lim}$ is the limit of the g_{net} of the RDCS in the DC voltage time scale, which is calculated when considering different stability margins of the DC voltage oscillation. In Fig. 18(a), $D_{\lim}$ is the limit of the DC voltage oscillation damping. For example, if $D_{\lim} = 0.1$, the stable region of g_{net} is indicated by the blue region in Fig. 18(a). The DC voltage oscillation is considered to be well damped if point (b_{net}, g_{net}) is located in this stable region. In addition, the traditional stable region of the operating states of the VSCs is calculated as shown in Fig. 18(b). This stable region is three-dimensional and thus, more complex than the stable region proposed in this study as shown in Fig. 19(a). It can be seen that if the output power of the VSCs is in the stable operating region in Fig. 18(b), the point (b_{net}, g_{net}) is located in the stable region in Fig. 18(a), and thus there is no problem of DC voltage oscillation. Compared with the traditional stable region, the stable region proposed in this study is simpler, as its dimension does not increase with the increase in the number of the VSCs. If there are too many VSCs in the

MTDC power system, the dimension of the traditional stable region may become too high to be used easily and visualized.

The following two study cases are presented to demonstrate the usefulness of calculating the proposed stable regions. At the steady state, the active power output from the slave VSCs respectively is 0.6, 0.2, and 0.1 p.u. If the output power of the 2nd VSC is to be increased to 0.75 p.u., it can be seen that the operating state of the VSCs is outside the stable region (red circles in Fig. 18), resulting in the oscillatory instability. A safe adjustment is to decrease the output power of the 3rd VSC to 0 p.u. at the same time. This ensures that the operating state continues to be located in the stable region (blue circles in Fig. 18) even if the output power of the 2nd VSC is increased to 0.75 p.u. The results of the nonlinear simulation to evaluate the two cases, when the active power of the 2nd VSC increases, are presented in Fig. 19.

Hence, the stable region proposed in this study can not only assist the stable power dispatching of the MTDC power system, but also is more convenient for power engineers to use than the traditional stable region based on active power outputs of the VSCs.

V. Conclusion

This study analyzed the stability of the DC voltage oscillation within an MTDC power system considering the system's comprehensive dynamics in the DC voltage time scale. It was demonstrated that ignoring parts of the dynamics of the MTDC power system can lead to missing some instability risks or errors in the analyzed results. The major contributions of this study are that it reveals the accurate stability mechanism of the DC voltage oscillation and provides a comprehensive understanding of the instability risk of DC voltage oscillations without ignoring any parts of the dynamics of the MTDC power system in the DC voltage time scale. The conclusions are as follows.

1) The determination of the collective impact of the RDCS on the DC voltage oscillation is clarified considering the comprehensive dynamics in a DC voltage time scale. If the equivalent conductance of the RDCS is negative, the damping of the DC voltage oscillation is reduced because the effect of the equivalent conductance and susceptance of the RDCS are both negative. If the equivalent conductance of the RDCS is positive, the collective effect of the RDCS should be determined by comparing the effect of the equivalent conductance and susceptance of the RDCS.
2) The accuracy of considering comprehensive dynamics of the MTDC power system in investigating DC voltage oscillation stability is verified. It is confirmed that simplifying the dynamics of the DC voltage control or ignoring the imaginary component of the RDCS can lead to errors in the conclusions or result in misestimating the instability risk of the DC voltage oscillation by analyzing the effect of power flow reversal and length of the transmission line on DC voltage oscillation stability, respectively.
3) A method of determining the stable operating region of the RDCS in the DC voltage time scale is proposed. Compared with the traditional stable region, the stable region proposed in this study has lower dimensions that does not increase with the increase in number of the VSCs. It is convenient for assisting engineers to avoid the instability risk of the MTDC power system even if much more dynamics are considered.
4) The proposed analysis method and obtained conclusions are effective for all of the MTDC power systems using master slave control and parts of the MTDC power systems using DC voltage droop control. The latter should satisfy the condition that DC voltage droop controlled VSCs can be written as a single-input and single-output transfer function and has one DC voltage oscillation mode. In this study, the effectiveness of the proposed analysis method and obtained conclusions in a DC voltage droop controlled MTDC power system with parallel connection is exanimated.

The MTDC power system using DC voltage droop control is complex if more general conditions are considered. Analyzing DC voltage stability of such a complex MTDC power system is a meaningful and challenge work. It will be conducted in-depth in the future.

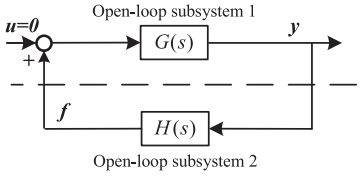

Fig. 20. Interconnected system.

Appendix A

A brief introduction of the open-loop modal resonance is as follows.

In Fig. 20, a closed-loop system consists of two open-loop subsystems. Let λ_g and λ_h denote oscillation modes of the open-loop subsystems $G(s)$ and $H(s)$, respectively. Let $\hat{\lambda}_g$ and $\hat{\lambda}_h$ denote the closed-loop oscillation modes corresponding to λ_g and λ_h, respectively. The differences between the closed-loop and open-loop oscillation modes are $\Delta\lambda_g = \hat{\lambda}_g - \lambda_g$ and $\Delta\lambda_h = \hat{\lambda}_h - \lambda_h$, which can be derived as follows.

The characteristic equation of the closed-loop system shown in Fig. 20 is

$$H(s)G(s) - 1 = 0 \tag{A1}$$

Let

$$G(s) = \frac{g(s)}{s - \lambda_g}, H(s) = \frac{h(s)}{s - \lambda_h} \tag{A2}$$

Substituting (A2) into (A1) gives

$$h(s)g(s) = (s - \lambda_g)(s - \lambda_h) \tag{A3}$$

If $\lambda_g = \lambda_h$, substituting $\hat{\lambda}_g$ into (A3), yields

$$\Delta{\lambda_g}^2 = h(\hat{\lambda}_g)g(\hat{\lambda}_g) \tag{A4}$$

From (A4), $\Delta\lambda_g$ is obtained as

$$\Delta\lambda_g = \pm\sqrt{h(\hat{\lambda}_g)g(\hat{\lambda}_g)} \tag{A5}$$

Thus, the closed-loop oscillation modes of the interconnected system can be obtained as

$$\hat{\lambda}_g = \lambda_g + \sqrt{h(\hat{\lambda}_g)g(\hat{\lambda}_g)}, \hat{\lambda}_h = \lambda_g - \sqrt{h(\hat{\lambda}_g)g(\hat{\lambda}_g)} \quad \text{(A6)}$$

It can be seen from (A6) that if λ_g equals to λ_h on the complex plane, $\hat{\lambda}_g$ and $\hat{\lambda}_h$ will move in opposite directions on the complex plane away from λ_g and λ_h, respectively, reducing stability of the system.

Regarding the mirrored systems in Fig. 5, the open-loop modes of which are same. It can lead to occurrence of the open-loop modal resonance and thus, one of the oscillation modes moves towards the right side of the complex plan. Consequently, the stability of the system is reduced.

APPENDIX B

TABLE I
PARAMETERS OF THE VSC-MTDC SYSTEM IN FIG. 7 AND FIG. 17

Parameters	Value (p.u.)
Direct voltage of the 1st VSC.	$V_{dc1} = 1.0$.
Input power of the 2nd VSC ~ 4th VSC.	$P_{s2} = 0.05, P_{s3} = 0.1, P_{s4} = 0.1$.
Capacitances of four VSCs.	$C_1 = C_2 = C_3 = 6.59$.
Control parameters of four VSCs.	K_{p1}=0.35 , K_{i1}=120/ω_0 , K_{p2}=0.1 , K_{i2}=20/ω_0 , K_{p3}=0.1 , K_{i3}=20/ω_0 , K_{p4}=0.1 , K_{i4}=20/ω_0 .
Impedance of the transmission lines. (Fig.7)	$z_1 = 0.0024 + j0.0045$, $z_2 = 0.024 + j0.045$, $z_3 = 0.048 + j0.089$, $z_4 = 0.072 + j0.135$.
Impedance of the transmission lines. (Fig.17)	$z_1 = 0.0024 + j0.0045$, $z_2 = z_7 = 0.024 + j0.045$, $z_3 = z_6 = 0.048 + j0.089$, $z_4 = 0.072 + j0.135$. $z_5 = 0.012 + j0.023$.

REFERENCES

[1] L. Huang, H. Xin, H. Yang, Z. Wang, and H. Xie, "Interconnecting very weak AC systems by multiterminal VSC-HVDC links with a unified virtual synchronous control," *IEEE J. Emerg. Sel. Topics Power Electron.*, vol. 6, no. 3, pp. 1041–1053, Sep. 2018.

[2] Z. Wang *et al.*, "A coordination control strategy of voltage-source-converter-based MTDC for offshore wind farms," *IEEE Trans. Ind. Appl.*, vol. 51, no. 4, pp. 2743–2752, Aug. 2015.

[3] W. Du, Y. Wang, and Y. Wang, H. F. Wang, and X. Xiao, "Analytical examination of oscillatory stability of a grid-connected PMSG wind farm based on the block diagram model," *IEEE Trans. Power Syst.*, vol. 36, no. 6, pp. 5670–5683, Nov. 2021.

[4] F. Zhang, H. Xin, D. Wu, Z. Wang, and D. Gan, "Assessing strength of Multi-infeed LCC-HVDC systems using generalized short circuit ratio," *IEEE Trans. Power Syst.*, vol. 34, no. 1, pp. 467–480, Jan. 2019.

[5] N. Chaudhuri, R. Majumder, B. Chaudhur, and J. Pan, "Stability analysis of VSC MTDC grids connected to multimachine AC systems," *IEEE Trans. Power Del.*, vol. 26, no. 4, pp. 2774–2784, Oct. 2011.

[6] W. Du, Q. Fu, and H. F. Wang, "Subsynchronous oscillations caused by open-loop modal coupling between VSC-based HVDC line and power system," *IEEE Trans. Power Syst.*, vol. 33, no. 4, pp. 3664–3677, Jul. 2018.

[7] W. Wang, M. Barnes, O. Marjanovic, and O. Cwikowski, "Impact of DC breaker systems on multiterminal VSC-HVDC stability," *IEEE Trans. Power Del.*, vol. 31, no. 2, pp. 769–779, Apr. 2016.

[8] M. K. Bucher, R. Wiget, and G. Andersson, "Multiterminal HVDC networks—What is the preferred topology?," *IEEE Trans. Power Del.*, vol. 29, no. 1, pp. 406–413, Feb. 2014.

[9] Q. Fu, W. Du, and H. F. Wang, "Planning of the DC system considering restrictions on small signal stability of EV charging stations and comparison between series and parallel connections," *IEEE Trans. Veh. Technol.*, vol. 69, no. 10, pp. 10724–10735, Oct. 2020.

[10] G. O. Kalcon, G. P. Adam, O. Anaya-Lara, S. Lo, and K. Uhlen, "Small-signal stability analysis of multi-terminal VSC-based DC transmission systems," *IEEE Trans. Power Syst.*, vol. 27, no. 4, pp. 1818–1830, Nov. 2012.

[11] L. Xiao, Z. Xu, T. An, and Z. Bian, "Improved analytical model for the study of steady state performance of droop-controlled VSC-MTDC systems," *IEEE Trans. Power Syst.*, vol. 32, no. 3, pp. 2083–2093, May 2017.

[12] L. Guo, P. Li, X. Li, F. Gao, D. Huang, and C. Wang, "Reduced-order modeling and dynamic stability analysis of MTDC systems in DC voltage control timescale," *CSEE J. Power Energy Syst.*, vol. 6, no. 3, pp. 591–600, Sep. 2020.

[13] H. Zhang, L. Harnefors, X. Wang, H. Gong, and J.-P. Hasler, "Stability analysis of grid-connected voltage-source converters using SISO modeling," *IEEE Trans. Power Electron.*, vol. 34, no. 8, pp. 8104–8117, Aug. 2019.

[14] X. Lu, K. Sun, J. M. Guerrero, J. C. Vasquez, L. Huang, and J. Wang, "Stability enhancement based on virtual impedance for DC microgrids with constant power loads," *IEEE Trans. Smart Grid*, vol. 6, no. 6, pp. 2770–2783, Nov. 2015.

[15] G. Pinares and M. Bongiorno, "Modeling and analysis of VSC-based HVDC systems for DC network stability studies," *IEEE Trans. Power Del.*, vol. 31, no. 2, pp. 848–856, Apr. 2016.

[16] Q. Fu, W. Du, and H. F. Wang, "Analysis of small-signal power oscillations in MTDC power transmission system," *IEEE Trans. Power Syst.*, vol. 36, no. 4, pp. 3248–3259, Jul. 2021.

[17] Q. Fu, W. Du, H. F. Wang, B. Ren, and X. Xiao, "Small-signal stability analysis of a VSC-MTDC system for investigating DC voltage oscillation," *IEEE Trans. Power Syst.*, vol. 36, no. 6, pp. 5081–5091, Nov. 2021.

[18] W. Du, Q. Fu, and H. F. Wang, "Damping torque analysis of DC voltage stability of an MTDC network for the wind power delivery," *IEEE Trans. Power Del.*, vol. 35, no. 1, pp. 324–338, Feb. 2020.

[19] W. Du, Q. Fu, and H. F. Wang, "Small-Signal stability of a DC network planned for electric vehicle charging," *IEEE Trans. Smart Grid*, vol. 11, no. 5, pp. 3748–3762, Sep. 2020.

[20] A. S. Matveev, J. E. Machado, and R. Ortega, J. Schiffer, and A. Pyrkin, "A tool for analysis of existence of equilibria and voltage stability in power systems with constant power loads," *IEEE Trans. Autom. Control*, vol. 65, no. 11, pp. 4726–4740, Nov. 2020.

[21] N. R. Chaudhuri and B. Chaudhuri, "Adaptive droop control for effective power sharing in multi-terminal DC (MTDC) grids," *IEEE Trans. Power Syst.*, vol. 28, no. 1, pp. 21–29, Feb. 2013.

[22] H. Yuan, X. Yuan, and J. Hu, "Modeling of grid-connected VSCs for power system small-signal stability analysis in DC-link voltage control timescale," *IEEE Trans. Power Syst.*, vol. 32, no. 5, pp. 3981–3991, Sep. 2017.

[23] Y. Huang, X. Zhai, J. Hu, D. Liu, and C. Lin, "Modeling and stability analysis of VSC internal voltage in DC-link voltage control timescale," *IEEE J. Emerg. Sel. Topics Power Electron.*, vol. 6, no. 1, pp. 16–28, Mar. 2018.

[24] Y. Li, L. Fan, and Z. Miao, "Stability control for wind in weak grids," *IEEE Trans. Sustain. Energy*, vol. 10, no. 4, pp. 2094–2103, Oct. 2019.

[25] J. Beerten, S. D'Arco, and J. A. Suul, "Identification and small-signal analysis of interaction modes in VSC MTDC systems," *IEEE Trans. Power Del.*, vol. 31, no. 2, pp. 888–897, Apr. 2016.

[26] Y. Che, J. Jia, J. Zhu, X. Li, Z. Lv, and M. Li, "Stability evaluation on the droop controller parameters of multi-terminal DC transmission systems using small-signal model," *IEEE Access*, vol. 7, pp. 103948–103960, 2019.

[27] W. Du, Q. Fu, and H. F. Wang, "Power system small-signal angular stability affected by virtual synchronous generators," *IEEE Trans. Power Syst.*, vol. 34, no. 4, pp. 3209–3219, Jul. 2019.

[28] W. Du, Q. Fu, and H. F. Wang, "Open-loop modal coupling analysis for a multi-input multi-output interconnected MTDC/AC power system," *IEEE Trans. Power Syst.*, vol. 34, no. 1, pp. 246–256, Jan. 2019.

[29] M. Amin, M. Zadeh, J. A. Suul, E. Tedeschi, M. Molinas, and O. B. Fosso, "Stability analysis of interconnected AC power systems with multi-terminal DC grids based on the Cigré DC grid test system," in *Proc. 3rd Renewable Power Gener. Conf. (RPG 2014)*, 2014, pp. 1–6.

[30] K. Rouzbehi, A. Miranian, J. I. Candela, A. Luna, and P. Rodriguez, "A generalized voltage droop strategy for control of multiterminal DC grids," *IEEE Trans. Ind. Appl.*, vol. 51, no. 1, pp. 607–618, Feb. 2015.

[31] Math Works, Inc., "Average model of a 100-kW grid-connected PV array," Jan. 2022. [Online]. Available: https://www.mathworks.com/help/physmod/sps/ug/average-model-of-a-100-kw-grid-connected-pv-array.html